ELSEVIER

Journal of Electron Spectroscopy and Related Phenomena 126 (2002) 125–132

JOURNAL OF ELECTRON SPECTROSCOPY and Related Phenomena

www.elsevier.com/locate/elspec

Electron–phonon coupling in W(110)-(1×1)H

Eli Rotenberg[a,*], S.D. Kevan[b]

[a]*Advanced Light Source, Lawrence Berkeley National Laboratory, Berkeley, CA 94720, USA*
[b]*Physics Department, University of Oregon, Eugene, OR 97403, USA*

Abstract

Recently, we reported high resolution angle-resolved photoemission measurements that indicated unusually strong coupling between adsorbate vibrations and a surface-localized electron state in the system W(110)-(1×1)H. We have now extended these measurements to probe the electron–phonon coupling strength as a function of position on the relevant Fermi contour. We find that the strength of the coupling is strongly dependent on Fermi wave vector, with the electron–phonon coupling constant λ varying between zero and ~0.8. Qualitatively, the strength of the coupling is related to the position of the surface band in the projected bulk band gap, and therefore to the degree of surface localization of the surface state wave function. Such effects should play an important role in all adsorbate vibronic interactions, since the vibrational modes are generally highly localized to the outermost surface layer. We discuss these results in relation to the surface phonon anomalies observed on this surface.

Keywords: W(110); Electron-phonon coupling; Kohn anomaly

1. Introduction

Since the pioneering theoretical work of Tossatti, much effort has been expended to understand the role of the electron–phonon interaction at surfaces and, more significantly, the role that it plays in driving surface and thin film reconstructions through a charge-density-wave-like mechanism [1,2]. The prototypical examples of surface reconstruction driven by the electron–phonon interaction are W(100) and Mo(100), which form c(2×2) and near c(2×2) incommensurate reconstructions at low temperature, respectively [3–6]. Even with the discovery of ultrathin metal film reconstructions that are apparently driven by electron–phonon coupling [7,8], however, the number of surface reconstructions that fit this CDW paradigm remains rather small. For a particular metallic surface to exhibit a CDW reconstruction requires at least two favorable factors: Strong underlying electron phonon coupling and good nesting of surface Fermi contours. Apparently, only a few simple metal surfaces and thin film systems combine these properties.

Due largely to evolutionary improvements in surface preparation and advanced instrumentation for angle-resolved photoemission (ARP), progress is being made in measuring both the strength of the underlying electron–phonon interaction at surfaces and the degree of nesting of Fermi contours of surface-localized states [9–16]. Early results from such efforts have produced some surprises. For example, the electron phonon coupling parameter (λ) for the clean Be(0001) surface was found to be much

*Corresponding author.
E-mail address: erotenberg@lbl.gov (E. Rotenberg).

0368-2048/02/$ – see front matter
PII: S0368-2048(02)00147-0

larger than for bulk beryllium metal [10–13]. We recently reported a similar measurement for W(110)-(1×1)H for which an adsorbate phonon mode at relatively high energy was found to be strongly coupled to a particular surface band [15]. In bulk media, these two parameters, the characteristic phonon energy and the underlying coupling strength, tend to be anticorrelated [17]. One manifestation of this anticorrelation is that it limits the superconducting transition temperature in traditional superconductors. The measured combinations for Be(0001) and W(110)-(1×1)H are anomalous compared to related bulk systems, leading to speculations (as yet unconfirmed) that these systems might support exotic surface superconductivity. Another interesting aspect of these results is that, using the momentum resolution inherent in ARP, we were able to investigate the electron–phonon coupling for different bands having separate Fermi contours, or even for a given band at different points on its Fermi contour. For example, on W(110)-(1×1)H, two separate bands that are split only by the spin–orbit interaction exhibit dramatically different electron–phonon coupling parameters due to their differing degrees of surface localization [15,18,19]. Such an incisive measure of the electron–phonon coupling strength for a *k*-resolved state in a particular band is obviously not possible using traditional bulk measurements, which normally provide Fermi-surface-averaged results.

The purpose of the present paper is to report measurements of the electron–phonon coupling strength for the W(110)-(1×1)H system at different points on the strongly coupled Fermi contour reported previously. The prime motivation for this experiment is that part of this contour is well-nested with its image on other sides the surface Brillouin zone (SBZ) and has therefore been implicated in driving very deep and narrow anomalies in the surface phonon dispersion relations [18,20–24]. This is a system where both the coupling and the nesting seem to be quite strong, yet a CDW-related reconstruction is not observed. Careful measurements of the coupling strength around the strongly coupled and well-nested contour are in order, and these are reported here. The next section describes our experimental techniques. In Section 3 we present our results and analyze them to deduce the *k*-dependent coupling strength around the coupled/nested contour. We summarize our findings in the final section.

2. Experimental procedures

The W(110) single crystal was cleaned by repeatedly heating to T=1000 K in 1×10^{-7} Torr of oxygen and subsequently annealing to T~2200 K to remove the oxide layer. The base pressure of the chamber was 1×10^{-10} Torr, which rose to 1×10^{-9} Torr briefly during flashing. Surface states were observed at T~120 K with angle-resolved photoemission using undulator-generated 100 eV photons at beamline 7.0 of the Advanced Light Source at Lawrence Berkeley National Laboratory. A Gamma-data SES-100 electron energy analyzer was used to measure angle resolved photoelectron energy distribution curves (EDC's) and momentum distribution curves (MDC's). This device is capable of detecting photoelectrons simultaneously over a range of momenta and kinetic energy with high resolution and good sampling in both directions. The total instrumental contribution to the energy resolution was about 40 meV and the angular resolution was about $\pm0.05°$, yielding a momentum resolution of better than 0.01 Å^{-1} at the 100 eV photon energy used in these measurements. The ability to measure MDC's with good sampling and statistics was crucial to the success of these measurements, since these intensity versus momentum plots allow precise extraction of quasiparticle dispersion relations without interference from the Fermi level cut-off. Hydrogen coverage was determined from calibrated measurements of the surface core level splitting [25]. In the present investigation, we present results only for the saturated surface where one hydrogen atom is adsorbed per surface tungsten atom.

3. Experimental results

Fig. 1 shows a gray-scale plot of the measured photoemission intensity within 40 meV (the instrumental resolution) of the Fermi energy (E_F) over a range of wave vectors that encompasses the strongly coupled and nested Fermi contour for W(110)-(1×1)H. These data were collected by hold-

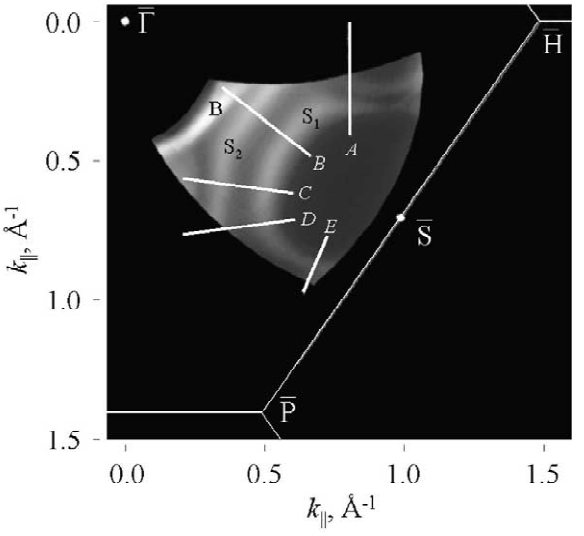

Fig. 1. Gray-scale plot of the photoemission intensity near the Fermi level for the W(110)-(1×1)H system. High intensity in white corresponds to regions where a band crosses the Fermi level and, therefore, to surface Fermi contours. The boundary of the nearby surface Brillouin zone boundary is shown, and the relevant Fermi orbit labeled S_1 is seen to be roughly elliptical in shape and to be centered at the $\bar{S}$ point. In later figures, we present and discuss quasiparticle dispersion relations along the lines labeled A–E.

ing the energy analyzer fixed in space and rotating the sample azimuthally to sweep the *k*-space region of the desired orbit through the analyzer window. Upon appropriate transformation, this procedure produces a three-dimensional data set of intensity as a function of parallel momentum and binding energy relative to the Fermi level. Compared to our earlier results [18], which were taken by sampling one angle at a time on a conventional, non-imaging analyzer, the present angular resolution is far superior, but there is also some slight, large-scale distortion of the overall map due to residual distortion associated with the electron-optical imaging system under the influence of stray fields in the apparatus. These do not affect the present analysis, which center on local effects near the Fermi crossings, as discussed below.

The constant-energy cut at the Fermi level shown in Fig. 1 produces experimental Fermi contours. The dominant feature in this case a roughly elliptical hole pocket with twofold symmetry about the $\bar{S}$ point of the SBZ. In previous papers, we have labeled the band that produces this orbit S_1 [18]. Portions of the Fermi contour of the spin–orbit split partner of this band (S_2) as well as the associated bulk (B) Fermi surface are visible near the periphery of Fig. 1. The nesting condition that leads to the deepest phonon anomaly, observed along the $\bar{\Gamma}\rightarrow\bar{H}=\bar{\Sigma}$ line [18,20–24], arises from coupling this S_1 orbit to the S_2 orbit associated with the mirror-related $\bar{S}$ point across the $\bar{\Gamma}\rightarrow\bar{N}=\bar{\Delta}$ line. Similarly, nesting of this S_1 orbit to the S_2 orbit associated with the opposite $\bar{S}$ point leads to a weaker phonon anomaly along the $\bar{\Gamma}\rightarrow\bar{S}$ line. Other regions of the orbit produce progressively less pronounced phonon anomalies, and no anomaly is observed near the $\bar{\Delta}$ line. The strength of a particular anomaly is related to both the degree of nesting, that is, the similarity in curvature of the relevant Fermi contours, and also to the underlying coupling matrix element between the electron gas and acoustic phonons at finite momentum. Based purely on the degree of nesting, it is not obvious why a related anomaly is not observed closer to the $\bar{\Delta}$ line in this system. The results presented below, which are related to the coupling strength between the electron gas and adsorbate optic phonons near zero momentum, shed some light on this issue.

By making a different cut through the aforementioned three-dimensional data set along particular lines in *k*-space, we can plot experimental quasiparticle dispersion relations, $\omega(\vec{k})$. We have analyzed data from 19 such cuts, 5 of which are indicated in Fig. 1. Gray-scale representations of slices A, B, C, D and E are shown in respective panels of Fig. 2. Smooth dispersion relations for S_1 and in some cases also for S_2 and B (not shown) are easily observed. To varying degrees, these smooth dispersions are interrupted by wiggles near the Fermi level that were previously shown to result from unusually strong coupling between the electron states and adsorbate phonons [15]. The wiggle is readily apparent for slice C, which lies close to the region of the contour that produces the strongest phonon anomaly along $\bar{\Sigma}$. The wiggle is less apparent in slice B, which lies close to the $\bar{\Gamma}\rightarrow\bar{S}$ line, and also in slice D. It is essentially absent from slices A and E, which lie nearer to the $\bar{P}\rightarrow\bar{H}$ SBZ boundary. This simple, qualitative observation already demonstrates the primary conclusion of this paper: the electron–phonon coupling strength is significantly wave-vec-

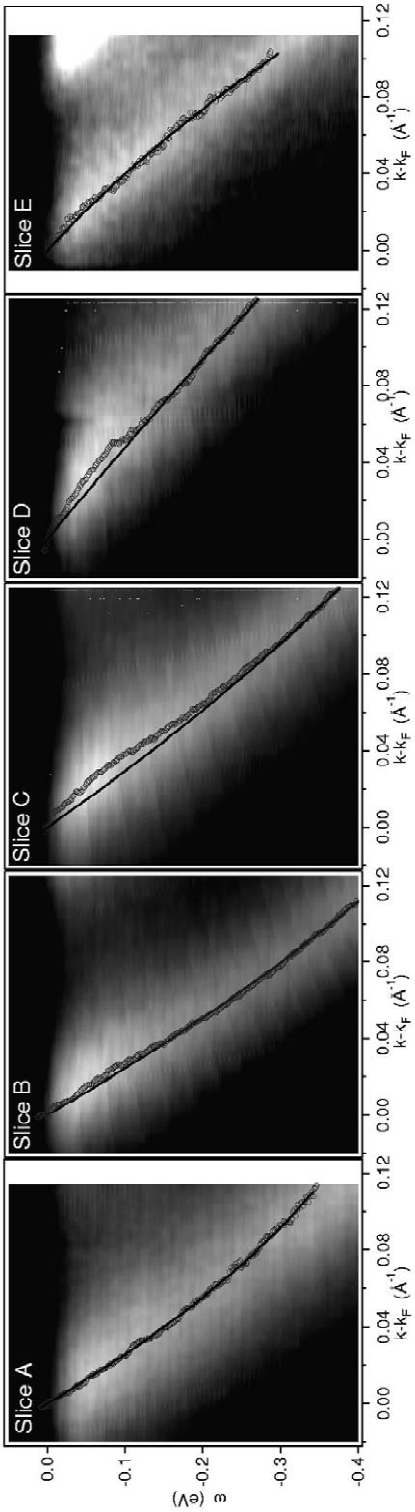

Fig. 2. Gray-scale plots of the quasiparticle dispersion relations along the slices A–E in Fig. 1. Open circles are fits to momentum distribution curves as explained in the text, and represent the fully dressed dispersion relation. The solid black lines are fits to the dispersion relations at high energy and correspond to what the dispersion relations would be in the absence of the electron–phonon coupling. The difference between these lines and the open circles corresponds to the real part of the electron–phonon self energy.

tor dependent and tends to be large near regions that support the strongest phonon anomalies and correspondingly reduced elsewhere on the Fermi orbit. Making horizontal cuts through these gray-scale plots produces MDC's: Intensity as a function of momentum (k) at constant quasiparticle energy ω. We find that the MDC's consist of nearly Lorentzian peaks for S_1, S_2, and B, with these peaks riding on a smooth, incoherent background. We numerically fitted these MDC's to Lorentzians convoluted with a minor Gaussian component related to the experimental momentum resolution, with a linear background added. The open circles superposed on the gray-scale images in Fig. 2 denote the peak positions derived from these fits. These circles are seen to reproduce the peak of the gray-scale image faithfully, and we take them to represent the fully dressed quasiparticle dispersion relations for the bands.

A good way to analyze such results is in terms of a many body complex electron–phonon self-energy function, $\Gamma(\omega)$. The real part of this function represents the deviation of the real quasiparticle dispersion relation from that for the non-interacting system, while the imaginary part corresponds to one half the of the inverse quasiparticle lifetime. In the present case, 'non-interacting system' refers to a hypothetical system in which the electron–phonon interaction is turned off, but other many body interactions such as the electron–electron interaction and impurity scattering are still operative [16]. Obviously, the dispersion relation for this hypothetical system cannot be measured. However, since other interactions operate on different energy scales, their impact at the Fermi level is essentially smooth and featureless. By contrast, the electron–phonon self-energy function is highly structured within a typical phonon energy of E_F, but is featureless far from E_F. Under these circumstances, it is a good approximation to set the 'non-interacting' band to the extrapolation of the quasiparticle band measured far from E_F. We fitted the quasiparticle band at $\omega > 0.3$ eV to a parabolic function constrained to pass through E_F, thereby ensuring that the real part of the self energy falls to zero at E_F, as required on general grounds. The resulting 'non-interacting' bands are indicated by the solid lines in Fig. 2. The difference between this band and the measured quasiparticle dispersion relation gives Re[$\Sigma(\omega)$] directly and is plotted for the same five k-space lines in Fig. 3.

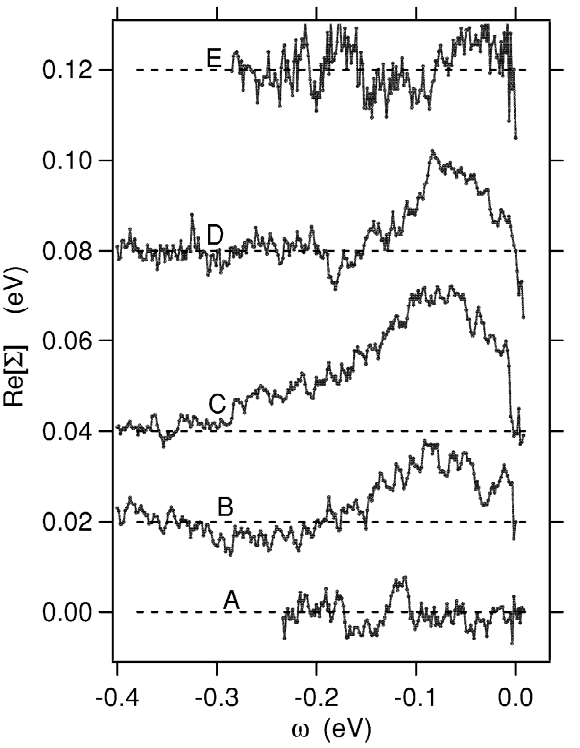

Fig. 3. Real part of the electron–phonon self energy, Re[Σ], as a function of energy near the Fermi level, along the k-space slices A–E in Fig. 1. Re[Σ] is large only for portions of the Fermi orbit where the surface band S_1 is relatively far from the bulk continuum and, therefore, relatively surface localized.

Before proceeding with a more detailed analysis, we first make some qualitative statements about the self-energy functions plotted in Fig. 3. Generally speaking, structure at a particular energy in the phonon density of states will be manifested by structure at the same energy in the electron–phonon self energy. In this adsorbate system, the phonon density of states near the surface consists of adsorbate 'optic branch' vibrations at relatively high energy as well as lower energy acoustic bulk and surface phonon modes [26,27]. The relevant energy scale in Fig. 3c is apparently of order 100 meV, an energy much higher than a typical acoustic phonon energy and, therefore, much higher than the tungsten Debye energy. In the previous paper, based on an analysis of EDC's only, we concluded that the dominant coupling is to the symmetric stretch adsorbate vibrational mode at 160 meV [15]. The present results generally support that notion, although the

peak in Re[$\Sigma(\omega)$] lies closer to 80–100 meV. It seems that the other lower-energy parallel hydrogen vibrations couple to the electronic degrees of freedom as well. The reason for the strong coupling between this surface band and the adsorbed hydrogen vibrational modes can be simply understood [16,28]. This band, which exists on the clean W(110) surface, shifts smoothly down in energy as hydrogen is adsorbed [29,30]. This downward shift implies that the band occupancy is a function of hydrogen coverage. We therefore expect that the occupancy is also a function of hydrogen position, so vibrations in the hydrogen layer lead to oscillating band occupancy, i.e., there might be strong electron–phonon coupling. Finally, we note the presence of a shoulder on the Re[$\Sigma(\omega)$] data at $\omega < 50$ meV. This shoulder, while very weak, is persistent regardless of the details of how we analyze data and it is observed to varying degrees for data collected around the Fermi contour. It is likely that this shoulder is caused by coupling to acoustic phonons, as was concluded on clean Be(0001) [10–13] and Mo(110) [14] without the 'interference' from the adsorbate 'optic' phonons. It is apparent that the electron–phonon self-energy in this system is as complex as the phonon density of states itself.

We now attempt to understand these data more quantitatively. Different approaches have been used to analyze similar data in the past. For clean Be(0001) [10–13] and Mo(110) [14], models for $\Sigma(\omega)$ based on a Debye spectrum of phonon states have been applied to extract a single electron phonon coupling parameter, λ. We previously tried without success to apply a related model using an Einstein phonon spectrum to our results for W(110)-(1×1)H [15]. A fundamental problem with these approaches is that they are derived from fairly simple phonon densities of states that cannot faithfully reproduce the complexity of the present system, as implied by the above discussion. Moreover, in simple models, the coupling parameter λ is generally derived by integrating over an entire electronic band. In the present case, our system apparently cannot be modeled with a simple phonon spectrum and the coupling is clearly not constant around even this single band with its simple elliptical Fermi contour. Indeed, our goal is to measure how specific *k*-selected states couple to the phonon bath and how this coupling varies around a single Fermi orbit. In the case where the coupling is independent of *k*, the well-known phonon-mediated renormalization of the Fermi velocity [31] is equivalent to the statement that the slope of Re[$\Sigma(\omega)$] at $\omega = 0$, is $-\omega$. We empirically generalize this notion to a set of individual points on the Fermi contour, thereby producing $\lambda(\vec{k}_F)$. We fitted the region between E_F and $\omega \sim 50$ meV to a straight line, and set the result to $-\lambda(\vec{k}_F)$.

Using this procedure, we find that the coupling constant λ attains its maximum values of 0.8 ± 0.2 near slice C. It falls to about one half this value at slices B and D, and is effectively zero at slices A and E. This newly measured value near the $\bar{\Gamma} \rightarrow \bar{S}$ line is somewhat lower than previously reported for this system, though comparable to the value reported for the analogous deuterium adsorption system [15]. The improved experimental momentum resolution and also the improved analysis technique based on MDC's rather than EDC's makes the current measurement more reliable. We have also tried to measure the coupling constant for the band S_2 using a similar procedure. As noted previously [15], this band is more weakly coupled than S_1, and we measure a maximum coupling of 0.2 ± 0.1 line and nearly zero otherwise. Previously, we attributed this smaller value of λ for S_2 relative to S_1 to the fact that S_2 lies closer to the bulk continuum and its wave function is consequently less surface localized. In similar fashion, we believe the primary reason why the coupling constant for S_1 varies so dramatically around the Fermi contour is that it closely approaches the bulk continuum as it crosses the SBZ boundary near the $\bar{P} \rightarrow \bar{H}$ line, and its wave function is less surface localized there. This can be qualitatively seen simply by projecting the bulk Fermi surface onto the surface Brillouin zone [32]: The surface Fermi contour on the hydrogen-covered surface threads its way through a very narrow gap in the bulk projection near $\bar{P} \rightarrow \bar{H}$, implying substantial delocalization from the surface in these regions of *k*-space. This means that the coupling to the highly surface-localized adsorbate vibrational modes is much reduced.

The electron–phonon coupling strength involving zero momentum adsorbate phonons is not necessarily related to that involving finite momentum acoustic phonons. Nonetheless, for this system, there is a

clear correspondence between Fermi level states that produce the deepest and shallowest phonon anomalies and those that are most strongly and weakly coupled to the hydrogen vibrations, respectively. This suggests a similar underlying phenomenon explains both observations. We therefore propose that the strength of the phonon anomaly is largely determined by the relative localization of the coupled surface bands, since the eigenvector of anomalous phonon mode is also fairly surface localized. While the existence of a phonon anomaly requires good nesting, electron–phonon coupling matrix elements play a significant role in determining the k-dependent strength of an anomaly. In the context of surface physics, a significant factor in determining these matrix elements is the spatial overlap between the surface state wave function and the phonon eigenvector.

The real and imaginary parts of $\Sigma(\omega)$ are Hilbert transforms of one another and, in principle, give similar information. The imaginary part is inversely related to the quasiparticle lifetime and directly related to the quasiparticle line width. We extracted these line widths from the MDC's. As expected, they show structure at energies comparable to the energy where structure is observed in the Re[$\Sigma(\omega)$]. The extracted linewidths are more statistically correlated than the peak position to how the incoherent background is included in the fit, so our results for Im[$\Sigma(\omega)$] are less accurate than those for Re[$\Sigma(\omega)$]. Moreover, the measured quasiparticle linewidths have a 'background' ~100 meV that probably arises from surface defect scattering and possibly also from scattering off acoustic phonons.

4. Conclusions

We have demonstrated that the electron phonon coupling constant in the W(110)-(1×1)H system depends markedly on which surface electron band is being considered and also on the location within each band. By itself, such a detailed k-resolved investigation of a many body interaction at a surface is very unusual and worthy of further investigation. Our results have implications beyond that simple observation:

- We noted in the previous article that the anomalous combination of large coupling strength and high characteristic phonon energy suggested that this surface might exhibit unusual surface superconductivity. Such predictions admittedly have had a very low success rate in the past even for bulk systems, and our present results indicate our prediction is unlikely to be observed. Only a small part of the Fermi orbit strongly coupled and that more weakly than was reported previously, so the driving force for the superconducting state will be consequently significantly reduced.
- Our results also fundamentally impact notions about vibronic coupling at surfaces in general and the role they play in adsorbate chemistry and photochemistry. Adsorbed particles interact most strongly with electron states in the outermost surface layer. The degree of surface localization of these states notably impacts their ability to affect nuclear motion and therefore needs to be carefully considered in attempts to understand surface chemistry at a very fundamental level of detail.
- Finally, our results suggest a new kind of surface spectroscopy, where, with higher resolution, lower temperature, and probably also a better surface preparation, the structure resolved in the self energy function will provide a very direct probe of which states are coupled to which vibrations and with what strength. Indeed, one limitation of our current results is that the impact of low energy acoustic modes on our spectral function.

Acknowledgements

This work was supported by the US DOE under grant DE-FG06-86ER45275 and was performed at the Advanced Light Source, supported by the US Department of Energy under contract DE-AC03-76SF00098.

References

[1] A. Fasolino, G. Santoro, E. Tosatti, Phys. Rev. Lett. 44 (1980) 1684.

[2] E. Tosatti, Solid State Commun. 25 (1978) 637.
[3] R.A. Barker, P.J. Estrup, F. Jona et al., Solid State Commun. 25 (1978) 375.
[4] M.K. Debe, D.A. King, Phys. Rev. Lett. 39 (1977) 708.
[5] M.K. Debe, D.A. King, Surface Sci. 81 (1979) 193.
[6] T.E. Felter, R.A. Barker, P.J. Estrup, Phys. Rev. Lett. 38 (1977) 1138.
[7] H.W. Yeom, S. Takeda, E. Rotenberg et al., Phys. Rev. Lett. 82 (1999) 4898.
[8] J.M. Carpinelli, H.H. Weitering, E.W. Plummer et al., Nature 381 (1996) 398.
[9] B.A. McDougall, T. Balasubramanian, E. Jenses, Phys. Rev. B 51 (1995) 13891.
[10] T. Balasubramanian, E. Jensen, X.L. Wu et al., Phys. Rev. B 57 (1998) R6866.
[11] S. LaShell, E. Jensen, T. Balasubramanian, Phys. Rev. B 61 (2000) 2371.
[12] M. Hengsberger, R. Fresard, D. Purdie et al., Phys. Rev. B 60 (1999) 10796.
[13] M. Hengsberger, D. Purdie, P. Segovia et al., Phys. Rev. Lett. 83 (1999) 592.
[14] T. Valla, A.V. Fedorov, P.D. Johnson et al., Phys. Rev. Lett. 83 (1999) 2085.
[15] E. Rotenberg, J. Schaefer, S.D. Kevan, Phys. Rev. Lett. 84 (2000) 2925.
[16] S.D. Kevan, E. Rotenberg, J. Elec. Spect. 117–118 (2001) 57.
[17] W.L. McMillan, Phys. Rev. 167 (1968) 331.
[18] E. Rotenberg, S.D. Kevan, Phys. Rev. Lett. 80 (1998) 2905.
[19] E. Rotenberg, S.D. Kevan, Phys. Rev. Lett. 82 (1998) 4066.
[20] E. Hulpke, J. Lüdecke, Surface Sci. 287/288 (1993) 837.
[21] B. Kohler, P. Ruggerone, S. Wilke et al., Phys. Rev. Lett. 74 (1995) 1387.
[22] B. Kohler, P. Ruggerone, S. Wilke et al., Zeitschrift f. Physikalische Chemie 197 (1996) 193.
[23] E. Hulpke, J. Lüdecke, Phys. Rev. Lett. 68 (1992) 2846.
[24] E. Hulpke, J. Lüdecke, Surface Sci. 272 (1992) 289.
[25] D.M. Riffe, G.K. Wertheim, P.H. Citrin, Phys. Rev. Lett. 65 (1990) 219.
[26] M. Balden, S. Lehwald, H. Ibach, Phys. Rev. B 53 (1996) 7479.
[27] M. Balden, S. Lehwald, E. Preuss et al., Surface Sci. 307–9 (1994) 1141.
[28] K.E. Smith, S.D. Kevan, Phys. Rev. Lett. 64 (1990) 567.
[29] R.H. Gaylord, K. Jeong, S.D. Kevan, J. Vac. Sci. Technol. A7 (1989) 2203.
[30] R.H. Gaylord, S.D. Kevan, Phys. Rev. B 37 (1988) 8491.
[31] N.W. Ashcroft, N.D. Mermin, Solid State Physics, Holt, Rinehardt, and Winston, New York, 1976.
[32] R.H. Gaylord, K. Jeong, S.D. Kevan, Phys. Rev. Lett. 62 (1989) 203.